Temperature-dependent electron-phonon spectral function and the intrinsic resistivity of a metal: A case study of monolayer Ti₂N

Binyuan Zhang, Mingfeng Zhu, Zhe Liu [ORCID], Fei Guo, and Yisong Zheng [ORCID]*

Key Laboratory of Physics and Technology for Advanced Batteries (Ministry of Education), Department of Physics, Jilin University, Changchun 130012, China

The transport spectral function of electron-phonon (e-ph) interaction in the double δ-function approximation (DDFA) is extensively employed to calculate the intrinsic resistivity (arising from e-ph scattering) of metallic materials in recent works of first-principles calculations. In contrast, a more fundamental transport spectral function with the Fermi smearing effect due to finite temperature (T) and nonzero phonon frequency is less involved. In this work, we perform first-principles calculations of the intrinsic resistivity of Ti₂N monolayer, a potential MXene material, by employing the two kinds of spectral function. We find that the spectral function with the DDFA fails to describe correctly the temperature dependence of the intrinsic resistivity of Ti₂N monolayer at $T > 250$ K, much lower than the Debye temperature. The underlying reason is that Ti₂N monolayer has a multisheet Fermi surface formed by several bands, and some band edges are very close to the Fermi surface. Our results suggest that the transport spectral function with the Fermi smearing effect, instead of the one with the DDFA, is always adequate for studying the intrinsic resistivity of realistic materials on the level of first-principles calculations. In addition, we give a brief remark on the intrinsic resistivity of Ti₂N monolayer, in contrast with other typical two-dimensional materials, which is significant from the viewpoint of application of such an MXene material.

I. INTRODUCTION

Electron-phonon (e-ph) interaction is an inevitable scattering mechanism to impede electronic transport in solids. In general, at and beyond room temperature, the resistivity or carrier mobility of solids is mainly limited by e-ph scattering [1,2]. The resistivity of a metal due to e-ph scattering is called the intrinsic resistivity (ρ). As an important electric transport property, the temperature dependence of intrinsic resistivity of metals is studied intensively from both experimental and theoretical standpoints [3–8]. According to conventional transport theory, when the temperature (T) exceeds the Debye temperature (T_D), the intrinsic resistivity of most metals exhibits a linear temperature dependence. For some metals with a very small Fermi surface, the linear temperature dependence of intrinsic resistivity comes about from a much lower temperature than T_D, called the Bloch-Grüneisen temperature (T_{BG}). It corresponds just to the thermal excitation temperature of the phonons, with the wave vector equal to the linear size of the Fermi surface. In the low-temperature limit, the intrinsic resistivity follows a power law of T^5 for three-dimensional (3D) and T^4 for two-dimensional (2D) systems, respectively [9]. However, for a realistic material, the ρ-T relation may deviate from these general rules largely due to the complicated Fermi surface or umklapp scattering processes, which are excluded from the conventional transport theory. In such a context, a first-principles calculation on the intrinsic resistivity of realistic metallic materials is highly desirable, which indicates a more detailed ρ-T relation than the above qualitative predictions.

Thus far, the electronic energy of a realistic material can be obtained numerically based on the density functional theory (DFT). In addition, the phonon frequency and the e-ph interaction matrix elements can be obtained by means of the density functional perturbation theory (DFPT) [10]. This progress involving first-principles calculations paves the way to study the intrinsic resistivity of a realistic metallic material, free from any empirical model. To calculate the intrinsic resistivity of a metal, the generalized Ziman resistivity formula is an adequate theoretical approach in which the resistivity is expressed in terms of a transport spectral function due to e-ph scattering [2], which is simply called a spectral function hereafter. An extensively used version of the spectral function in the literature is in the form of the so-called double δ-function approximation (DDFA) [3–5]. By means of such an approximation, the initial and final electronic states of e-ph scattering are both strictly restricted on the Fermi surface. In fact, without employing the DDFA, one can work out a more fundamental expression of the spectral function that becomes temperature-dependent, arising from the Fermi distribution of electrons around the Fermi level. However, such a temperature-dependent spectral function is employed less often to study the intrinsic resistivity of metals than its DDFA counterpart, though it means fewer restrictions to the electron and phonon states involved in the e-ph scattering. To obtain the intrinsic resistivity of realistic metallic materials with high

————————
*Author to whom all correspondence should be addressed: zhengys@jlu.edu.cn

precision from first-principles calculations, one must compare the intrinsic resistivity of metal calculated by the two kinds of spectral functions, with the aim of checking the validity of the spectral function within the DDFA as is used for studying the intrinsic resistivity of realistic metallic materials.

In this work, we perform first-principles calculation on the intrinsic resistivity of Ti_2N monolayer, a potential member of the MXene family from recent theoretical predictions [11–19]. Our numerical results indicate that with the increase in temperature, the intrinsic resistivity of Ti_2N monolayer exhibits two separate regions of linear temperature dependence. The first one occurs within 70–250 K, which is much lower than the Debye temperature ($T_D = 781$ K), while the onset temperature of the second linear temperature dependence region is about 1400 K, far larger than T_D. From these results, it seems that the linear temperature dependence of the intrinsic resistivity of Ti_2N monolayer is irrelevant to Debye temperature. This is at odds with the conventional transport theory. We find that these features of intrinsic resistivity of Ti_2N monolayer are closely associated with the temperature-dependent spectral function. In contrast, the spectral function of DDFA cannot correctly describe the temperature dependence of the intrinsic resistivity of Ti_2N monolayer. Beyond room temperature (300 K), it gives a numerical result that is remarkably different from that calculated by the temperature-dependent spectral function. The discrepancy of the intrinsic resistivity calculated by the two kinds of spectral functions implies that the DDFA fails to apply to the spectral function of Ti_2N monolayer. And the underlying reason is due to the appearance of some band edges within an energy shell around the Fermi level on the scale of $k_B(T_D + T)$. Such a case is expected to occur often in realistic materials with a multisheet Fermi surface, not limited only to Ti_2N monolayer. Therefore, much attention should be paid to such an issue when employing the DDFA to calculate the spectral function and further the intrinsic resistivity of realistic materials on the level of first-principles calculations.

The rest of this work is organized as follows. In Sec. II, we give a brief description of the theoretical methods, including the Ziman resistivity formula for calculating the intrinsic resistivity and the technical details of the first-principles calculations. In Sec. III, the numerical results of the intrinsic resistivity of Ti_2N monolayer are shown and discussed. Finally, in Sec. IV the main results are summarized.

II. THEORETICAL APPROACH AND COMPUTATIONAL METHODS

A. Ziman resistivity formula

In this work, we employ the Ziman formula [2] to calculate the intrinsic resistivity of Ti_2N monolayer. It was first derived by Ziman from the variational solution of the Boltzmann transport equation in the presence of e-ph scattering. Then, it was generalized by Allen to more realistic cases such as the complicated Fermi surface formed by multiple bands [20]. Thus, the Ziman resistivity formula becomes an appropriate approach for calculating the intrinsic resistivity of realistic metallic materials on the level of first-principles calculations. According to Allen's original work [21], the Ziman formula

expresses the intrinsic resistivity along a given direction, say the x direction, in terms of the spectral function. It takes the form

$$\rho_x = \frac{\pi}{e^2 \hbar N(E_f)\langle v_x^2 \rangle} \int d\Omega\, \alpha^2 F_T(\Omega)\mathcal{F}(k_B T/\Omega), \quad (1)$$

with

$$\mathcal{F}(k_B T/\Omega) = \frac{\Omega}{k_B T} \sinh^{-2}\left(\frac{\Omega}{2k_B T}\right). \quad (2)$$

And the spectral function is defined as

$$\alpha^2 F_T(\Omega) = \frac{1}{N_k N_q N(E_f)} \sum_{\substack{mnk \\ \nu q}} \frac{\delta(\Omega - \omega_{\nu q})}{\omega_{\nu q}} \left| \mathcal{G}_{mn}^\nu(\mathbf{k}, \mathbf{q}) \right|^2$$

$$\times \delta(E_{m\mathbf{k}+\mathbf{q}} - E_{n\mathbf{k}} - \hbar\omega_{\nu q})$$

$$\times (f_{n\mathbf{k}} - f_{m\mathbf{k}+\mathbf{q}})\left[1 - \frac{\mathbf{v}_{n\mathbf{k}} \cdot \mathbf{v}_{m\mathbf{k}+\mathbf{q}}}{|\mathbf{v}_{n\mathbf{k}}||\mathbf{v}_{m\mathbf{k}+\mathbf{q}}|} \right]. \quad (3)$$

In the above expressions, N_k and N_q are the numbers of $\mathbf{k}$ and $\mathbf{q}$ points of the Brillouin zone (BZ) sampling, respectively; $N(E_f)$ stands for the electronic density of states at the Fermi energy E_f. $\mathcal{G}_{mn}^\nu(\mathbf{k}, \mathbf{q})$ is the e-ph interaction matrix element between an electronic initial state $|n\mathbf{k}\rangle$ and a final state $|m\mathbf{k} + \mathbf{q}\rangle$ that is caused by emitting or absorbing a phonon of state $|\nu\mathbf{q}\rangle$. Note that n, m, and ν denote the indexes of electron bands and the phonon mode, respectively. $\omega_{\nu q}$ is the phonon frequency of the phononic state $|\nu\mathbf{q}\rangle$; $E_{n\mathbf{k}}$ and $E_{m\mathbf{k}+\mathbf{q}}$ are the electronic energy of the electronic states $|n\mathbf{k}\rangle$ and $|m\mathbf{k} + \mathbf{q}\rangle$, respectively. $f_{n\mathbf{k}}$ and $f_{m\mathbf{k}+\mathbf{q}}$ denote the Fermi distributions at these electronic states. $\mathbf{v}_{n\mathbf{k}}$ and $\mathbf{v}_{m\mathbf{k}+\mathbf{q}}$ are the band velocities [2,22]. $\langle v_x^2 \rangle$ denotes a squared average of the x-component of electronic velocity on the Fermi surface,

$$\langle v_x^2 \rangle = \frac{\sum_{n\mathbf{k}} (\mathbf{v}_{n\mathbf{k}} \cdot \mathbf{e}_x)^2 \delta(E_{n\mathbf{k}} - E_f)}{\sum_{n\mathbf{k}} \delta(E_{n\mathbf{k}} - E_f)}. \quad (4)$$

We have to point out that in Allen's original work, the spectral function is defined in an alternative form, i.e.,

$$\alpha^2 \tilde{F}_T(\Omega)$$

$$= \frac{1}{N_k N_q N(E_f)} \sum_{\substack{mnk \\ \nu q}} \delta(\Omega - \omega_{q\nu})\left| \mathcal{G}_{mn}^\nu(\mathbf{k}, \mathbf{q}) \right|^2 \delta(E_{n\mathbf{k}} - E_f)$$

$$\times \delta(E_{m\mathbf{k}+\mathbf{q}} - E_f)\left[1 - \frac{\mathbf{v}_{n\mathbf{k}} \cdot \mathbf{v}_{m\mathbf{k}+\mathbf{q}}}{|\mathbf{v}_{n\mathbf{k}}||\mathbf{v}_{m\mathbf{k}+\mathbf{q}}|} \right]. \quad (5)$$

Due to the appearance of two δ-functions on the right-hand side of the above expression, it is often referred to as the spectral function in the DDFA [23]. In comparison with the expression of the spectral function given by Eq. (3), the spectral function in the DDFA is used more extensively in studying the intrinsic resistivity of metallic materials on the level of first-principles calculations in recent relevant works [3–5]. However, it should be emphasized that Eq. (3) is the fundamental definition of the spectral function. In contrast, the DDFA introduces the excessive restriction that the electronic initial and final electronic states in the e-ph scattering process are completely confined on the Fermi surface. Consequently, the so-called Fermi smearing effect due to the nonzero phonon

energy and finite temperature is fully omitted, which must influence the calculated intrinsic resistivity to some extent. In fact, if we insert the identity $\int d\varepsilon \, \delta(\varepsilon - E_{nk}) = 1$ into Eq. (3), we then get

$$
\begin{aligned}
\alpha^2 F_T(\Omega) &= \int_{-\infty}^{\infty} d\varepsilon \frac{f(\varepsilon) - f(\varepsilon + \Omega)}{\Omega} I(\varepsilon, \Omega) \\
&\approx \int_{-\infty}^{\infty} d\varepsilon \left(-\frac{\partial f}{\partial \varepsilon}\right) I(\varepsilon, \Omega) \\
&\approx \alpha^2 \tilde{F}_T(\Omega) + \frac{\pi^2}{6} (k_B T)^2 \frac{\partial^2 I(\varepsilon, \Omega)}{\partial^2 \varepsilon}\bigg|_{\varepsilon = E_f}
\end{aligned} \quad (6)
$$

with

$$
\begin{aligned}
I(\varepsilon, \Omega) &= \frac{1}{N_k N_q N(E_f)} \sum_{\substack{mnk \\ vq}} \delta(\Omega - \omega_{vq}) \left| \mathcal{G}_{mn}^{v}(\boldsymbol{k}, \boldsymbol{q}) \right|^2 \\
&\times \delta(E_{mk+q} - E_{nk} - \hbar\omega_{vq}) \\
&\times \delta(\varepsilon - E_{nk}) \left[1 - \frac{\boldsymbol{v}_{nk} \cdot \boldsymbol{v}_{mk+q}}{|\boldsymbol{v}_{nk}||\boldsymbol{v}_{mk+q}|} \right].
\end{aligned} \quad (7)
$$

It is not difficult to infer that the prerequisites from the second step to the third step of Eq. (6) are $E_f \gg k_B T_D$ and $E_f \gg k_B T$. It must be emphasized that E_f herein just refers to the difference between the Fermi energy and the proximate band edge. Besides, to reach the last result from the third step of Eq. (6), use has been made of the Sommerfeld expansion. To sum up, from the above analysis we can conclude that the validity of the DDFA applied to the spectral function consists of the following aspects: the Fermi energy is much larger than the thermal excitation energy and phonon Debye energy. Meanwhile, the function $I(\varepsilon, \Omega)$ versus ε is slowly varying in the vicinity of the Fermi energy. Usually, $I(\varepsilon, \Omega)$ is deemed to be mainly determined by the electronic density of states around the Fermi energy, whereas the e-ph interaction matrix element and the term for the large-angle scattering weight do not change very much, although this is never demonstrated formally. However, for realistic metallic materials, it is often difficult to identify whether these preconditions hold true. For example, in the case of a complicated Fermi surface formed by multiple bands, the Fermi energy is very close to the edges of one or several bands; however, far away from the edges of other bands, the Fermi level spans all of these bands. Consequently, it is not straightforward to estimate whether the Fermi energy is much larger than the thermal excitation energy and phonon Debye energy. It will be seen that such a situation occurs in Ti$_2$N monolayer, a potential MXene material under our consideration for calculating the intrinsic resistivity on the level of first-principles calculations. Therefore, the applicability of the DDFA to the spectral function is doubtful, although it is used extensively in relevant works.

If the transport spectral function is decomposed into mode-resolved ingredients as $\alpha^2 F_T(\Omega) = \sum_v \alpha^2 F_T^v(\Omega)$, then the resistivity can be written as the summation of the contributions of each phonon mode to the intrinsic resistivity, i.e.,

$$
\rho_x = \sum_v \rho_x^v. \quad (8)
$$

If the summation over v on the right side of the above equation is restricted within the acoustic phonon (AP) and optical phonon (OP) modes, respectively, we can obtain the individual contributions of acoustic and optical modes to the intrinsic resistivity, denoted as ρ_x^{AP} and ρ_x^{OP}, respectively. Then, we define $\kappa^{AP} = \rho_x^{AP}/\rho_x$ and $\kappa^{OP} = \rho_x^{OP}/\rho_x$, which stand for the respective percentages of the contributions of acoustic and optical modes to the intrinsic resistivity. By the same token, we can divide the spectral function into two parts of the acoustic and optical phonon modes, denoted as $\alpha^2 F_T^{AP}(\Omega)$ and $\alpha^2 F_T^{OP}(\Omega)$, respectively. These quantities will be used to analyze the numerical results of the intrinsic resistivity of Ti$_2$N monolayer.

B. Computational methods

To investigate the intrinsic resistivity of Ti$_2$N monolayer on the level of first-principles calculations, detailed knowledge about the electronic and phononic states and e-ph interaction matrix elements is required. The calculations for these quantities are performed in the theoretical frameworks of DFT and DFPT, respectively, by using the QUANTUM ESPRESSO package [24]. In addition, we adopt the norm-conserving pseudopotential [25] to model the ionic potential and the generalized gradient approximation (GGA) of the Perdew-Burke-Ernzerhof (PBE) functional [26] for the exchange-correlation interaction. A coarse Monkhorst-Pack [27] $10 \times 10 \times 1$ mesh is employed to sample both $\boldsymbol{k}$ points and $\boldsymbol{q}$ points in the BZ.

The aforementioned numerical results do not suffice for exploring the intrinsic resistivity of Ti$_2$N monolayer quantitatively because the $\boldsymbol{k}$-mesh and $\boldsymbol{q}$-mesh are both too coarse to result in an accurate description of the e-ph scattering processes in the vicinity of the Fermi surface. However, first-principles calculations on a much finer $\boldsymbol{k}$-mesh or $\boldsymbol{q}$-mesh imply a formidable computational burden. To circumvent such a prohibitive task, we adopt a generalized Fourier interpolation approach realized by the EPW code [28] in real space, which enables affordable and accurate calculations of the electronic and phonon energy spectra as well as the e-ph coupling on ultrafine $\boldsymbol{k}$-mesh and $\boldsymbol{q}$-mesh.

III. RESULTS AND DISCUSSIONS

A. Structure and electronic properties

Before performing the numerical calculations on the intrinsic resistivity, it is significant to outline the crystal structure and the electronic and phononic dispersions of Ti$_2$N monolayer. Such a potential MXene material has a hexagonal crystal structure. Its lattice structure and BZ with the Fermi surface embedded in it are illustrated in Fig. 1. After a full relaxation calculation, we obtain that the lattice constant of Ti$_2$N is $a_1 = a_2 = a = 3.03$ Å, and the thickness of the Ti$_2$N triple atomic layers is 2.39 Å with a Ti-N bond length of 2.12 Å. The electronic band structures of Ti$_2$N obtained by DFT (blue solid line) and Wannier interpolation (black dashed line) along the high-symmetry path are shown in Fig. 2(a). Both of them give the same energy spectrum in the energy range of 2 eV around the Fermi energy taken as zero energy. From the electronic band structure, we can see that more
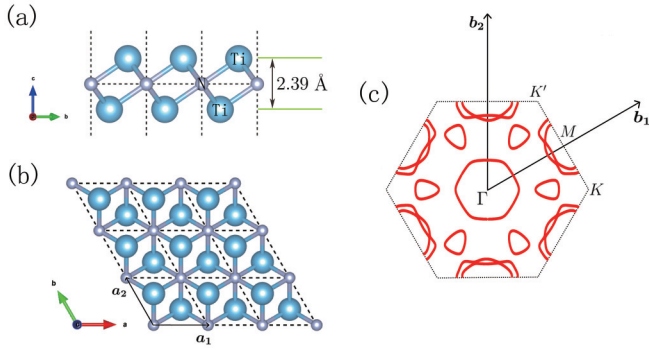
FIG. 1. (a) Side view and (b) top view of the Ti_2N monolayer. In (b) a_1 and a_2 are the lattice vectors of Ti_2N monolayer, and the unit cell of Ti_2N lattice is shown by a dashed line. (c) Brillouin zone of Ti_2N with the Fermi surface embedded in it, high-symmetry points labeled; b_1 and b_2 are the inverse lattice vectors.

than one band spans the Fermi level, hence the Fermi surface of Ti_2N monolayer has a multibranch profile, as seen in Fig. 1(c). It is noteworthy the some band edges are very close to the Fermi level. For example, at the small electron and hole pockets marked in Fig. 2(a), the differences between the band edges and the Fermi level are 83 and 87 meV, respectively. They are not much larger than the Debye energy (67 meV) as given below. Such a band feature may prevent the DDFA from applying to the Ti_2N monolayer to calculate the intrinsic resistivity. Phononic dispersion of Ti_2N monolayer along the high-symmetry path with no imaginary frequency is presented in Fig. 2(b). There are nine phonon modes in Ti_2N monolayer, including three acoustic branches ($\nu = 1$–3) and six optical branches ($\nu = 4$–9). The calculated maximal phonon frequency on the q-mesh is about 550 cm^{-1}, which can be viewed as the Debye frequency ω_D. And one can get the Debye temperature by using $k_B T_D = \hbar \omega_D$ [29]. The corresponding Debye temperature is $T_D = 781$ K, and the corresponding Debye energy is 67 meV. In addition, from Fig. 2(b) it is obvious that the frequencies of acoustic modes are globally lower than the optical modes. As shown below, such a feature plays a critical role in determining the temperature dependence of the intrinsic resistivity.

B. Intrinsic resistivity

With the theoretical approaches presented above, we are now in the position to perform numerical calculations on the intrinsic resistivity of Ti_2N monolayer on the level of first-principles calculations. To do this, we will employ the two kinds of spectral functions given by Eqs. (3) and (5), respectively. The former ($\alpha^2 F_T$) is fundamental and temperature-dependent, while the latter ($\alpha^2 \tilde{F}_T$) is the result of the DDFA. Our main aim is to check the validity of the DDFA adopted frequently in the literature to study the intrinsic resistivity of metallic materials. With the help of the Wannier interpolation technique, we can take much fine BZ samplings to treat the k and q integrations numerically in order to calculate the intrinsic resistivity with high precision. To perform numerical calculations, the Dirac δ-function in the spectral function is approximated by the Gaussian smearing
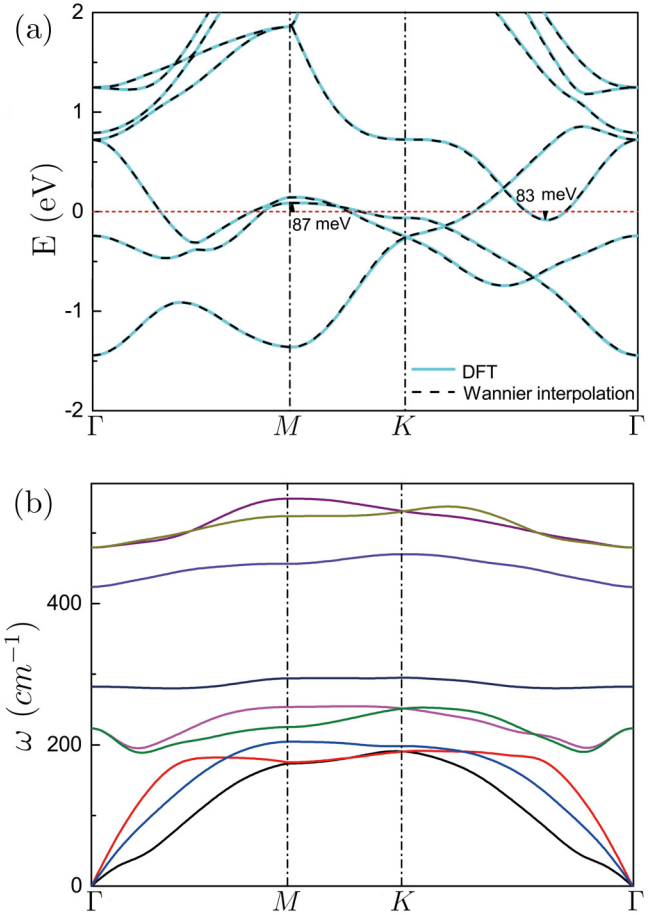
FIG. 2. (a) Electronic and (b) phononic dispersions of Ti_2N monolayer along the high-symmetry path Γ-M-K-Γ. The electronic band structures of Ti_2N monolayer obtained by DFT (blue solid line) and Wannier interpolation (black dashed line) along the high-symmetry path are exhibited in (a). Fermi energy is shifted to be 0 eV. The difference between the band edge of the small electron (hole) pockets and the Fermi level is 83 meV (87 meV). The phonon modes ordered by frequency are identified by magnitude from 1 (the lowest) to 9 (the highest). The three phonon modes with zero frequency at the high-symmetry point Γ are acoustic branches ($\nu = 1$–3), and the remaining six are optical branches ($\nu = 4$–6).

function with a broadening σ. The convergence of the intrinsic resistivity calculated by $\alpha^2 F_T$ with respect to the density of BZ sampling and the Gaussian broadening is shown in Fig. 3(a). We find that at room temperature (300 K), $200 \times 200 \times 1$ k-mesh and q-mesh with an appropriate Gaussian broadening $\sigma = 5 \times 10^{-4}$ eV can yield the convergent result of intrinsic resistivity. In comparison with the result obtained with much finer k-mesh and q-mesh, the relative error of the obtained intrinsic resistivity is less than 1%. In addition, even at very low temperature, i.e., 20 K, our numerical calculations indicate that such fine ($200 \times 200 \times 1$) k-mesh and q-mesh are sufficient to result in a convergent intrinsic resistivity with a relative error less than 1%. In contrast, the convergence of the intrinsic resistivity calculated by $\alpha^2 \tilde{F}_T$ is also checked, and the numerical results are shown in Fig. 3(b). It can be seen that if we adopt the Gaussian broadening $\sigma = 5 \times 10^{-4}$ eV, we need at least $1600 \times 1600 \times 1$ k- and q-mesh to guarantee the
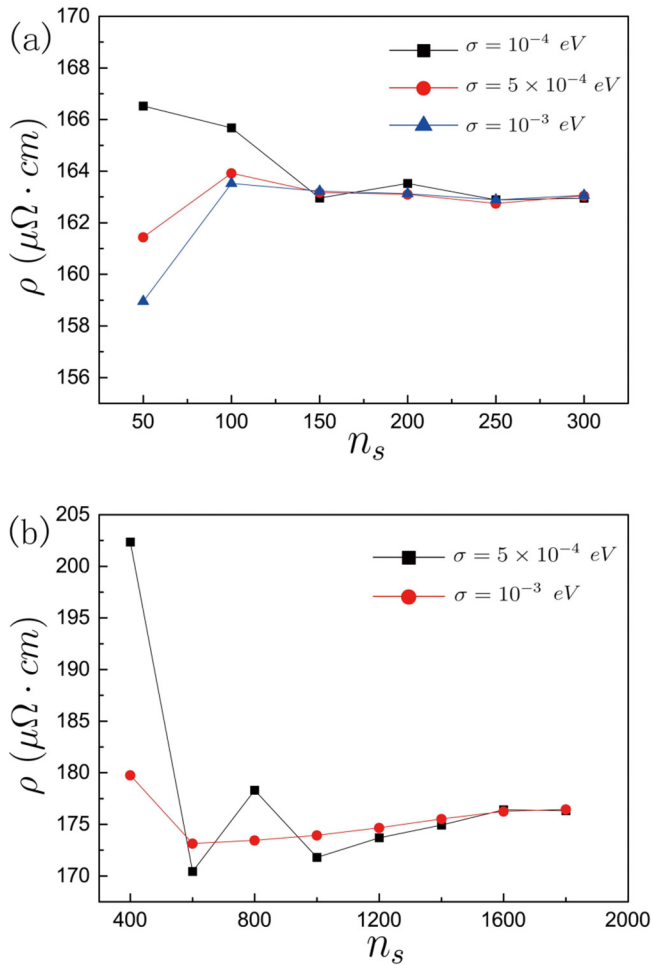
FIG. 3. Intrinsic resistivity of Ti$_2$N monolayer with varied Gaussian broadening parameter σ and $n_s \times n_s \times 1$ **k**- and **q**-mesh calculated by (a) $\alpha^2 F_T$ and (b) $\alpha^2 \tilde{F}_T$. All results are calculated at 300 K.

FIG. 4. The variation of ρ_θ / ρ_x with angle θ. ρ_θ is the intrinsic resistivity driven by the electric field in the direction with the angle θ with respect to the x-axis. This result is calculated by $\alpha^2 F_T$ at 300 K.

convergence of the numerical results [the relative error of the obtained intrinsic resistivity in Fig. 3(b) is less than 1%]. This implies that the convergence of the numerical results becomes more difficult when the DDFA is employed in the spectral function. After the convergence test, we study the anisotropy of the intrinsic resistivity of Ti$_2$N monolayer at room temperature (300 K). As shown in Fig. 4, the variation of ρ_θ / ρ_x with angle θ is plotted. ρ_θ is the intrinsic resistivity driven by the electric field in the direction with the angle θ with respect to the x-axis. The result indicates that the anisotropy of Ti$_2$N monolayer is very small (ρ_θ / ρ_x is 0.957 at the minimum) and can be ignored. Based on this result, below we will only focus on the intrinsic resistivity along the x-direction.

First of all, we are interested in the temperature dependence of the intrinsic resistivity of Ti$_2$N monolayer. The numerical results are shown in Fig. 5. As shown in Fig. 5(a), below 45 K, the intrinsic resistivities calculated by the two kinds of spectral functions are quantitatively consistent. An important feature of the intrinsic resistivity spectrum in such a low-temperature region is that ρ is proportional to T^4, which is a universal result of the intrinsic resistivity of 2D metals in the low-temperature limit predicted by the conventional

transport theory [9]. Then, the numerical result of the intrinsic resistivity of Ti$_2$N monolayer calculated by $\alpha^2 F_T$ in the subsequent wide temperature region (50–2000 K) is shown in Fig. 5(b). This numerical result indicates that with the increase of temperature, the intrinsic resistivity of Ti$_2$N monolayer calculated without the DDFA exhibits two separate regions of a linear temperature dependence. The first one occurs within 70–250 K, which is much lower than the Debye temperature ($T_D = 781$ K), while the onset temperature of the second linear temperature dependence region is about 1400 K, far larger than T_D. According to conventional transport theory, when the temperature exceeds the Debye temperature, all of the phonons are fully thermally excited, with the average phonon number being about T/T_D. Considering that the e-ph scattering rate is proportional to the average phonon number, a straightforward conclusion is that the linear ρ-T relation holds at and beyond the Debye temperature. However, our numerical result shown in Fig. 5(b) is at odds with such a prediction of conventional transport theory. It seems that the appearance of both linear ρ-T regions of Ti$_2$N monolayer is not directly associated with T_D since they occur in either much lower or higher temperature regions than T_D. In contrast to the result shown in Fig. 5(b), the temperature dependence of the intrinsic resistivity of Ti$_2$N monolayer calculated by $\alpha^2 \tilde{F}_T$ in the temperature range from 50 to 2000 K is shown in Fig. 5(c). We can see that the DDFA brings about a distinct result. Namely, the linear ρ-T relation always holds true in the temperature range of 70–2000 K. Moreover, a detailed comparison of the intrinsic resistivity calculated by the two kinds of spectral functions within 50–2000 K is plotted in Fig. 5(d). Below 250 K, the results obtained by the two spectral functions are in good agreement. But the difference between the two results becomes sizable as the temperature increases gradually. Even at room temperature (300 K), the relative difference between them amounts to 8.2%.

It is now necessary to give a reasonable explanation of the temperature dependence of the intrinsic resistivity of Ti$_2$N monolayer as shown Fig. 5(b). To begin with, by means of the Ziman formula we try to explain the untimely occurrence of
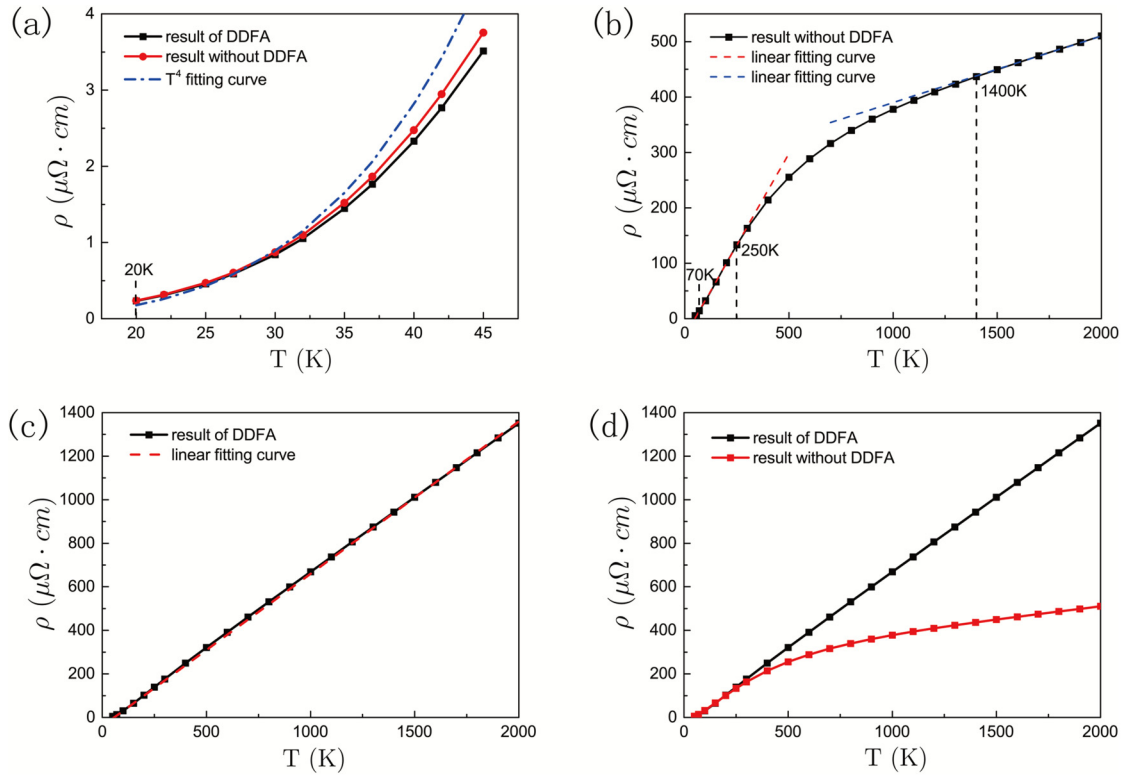
FIG. 5. (a) Resistivity of Ti_2N monolayer calculated by $\alpha^2\tilde{F}_T$ (black solid line) and α^2F_T (red dashed line) vs temperature T within 20–45 K, with the T^4 fitting curve plotted for comparison. Resistivity of Ti_2N calculated by (b) α^2F_T and (c) $\alpha^2\tilde{F}_T(\Omega)$ vs temperature T within 50–2000 K, with the linear fitting curve plotted for comparison. (d) Resistivity of Ti_2N monolayer calculated by $\alpha^2\tilde{F}_T$ (black solid line) and α^2F_T (red dashed line) vs temperature T within 50–2000 K.

the linear temperature dependence of the calculated intrinsic resistivity from 70 to 250 K as shown in Fig. 5(b), which is much lower than T_D. According to the expressions given by Eqs. (1)–(3), the temperature dependence of the intrinsic resistivity comes from the spectral function $\alpha^2F_T(\Omega)$ as well as the function $\mathcal{F}(x)$. They are associated with the temperature dependence of the electron and phonon distributions, respectively. And their profiles are plotted in Figs. 6(a) and 6(b), respectively. As shown in Fig. 6(a), the spectral function $\alpha^2F_T(\Omega)$ hardly changes with temperature within 50–250 K. And they do not show a nontrivial difference from the result of the DDFA. This implies that the temperature dependence of intrinsic resistivity is solely determined by the function $\mathcal{F}$ in such a low-temperature region. As shown in Fig. 6(b), the function $\mathcal{F}(T/T_0)$ starts to show the linear temperature dependence from a critical temperature of about $0.22T_0$ with T_0 as a characteristic temperature. Let us now digress for a moment to have a look at Fig. 6(c), which displays the phonon distribution function $\mathcal{N}(T/T_0) = 1/[\exp(T_0/T) - 1]$. The function $\mathcal{N}(T/T_0)$ begins to exhibit a linear temperature dependence for a critical temperature of about $0.5T_0$. According to conventional transport theory, the intrinsic resistivity is simply proportional to the e-ph scattering rate. And the e-ph scattering rate is proportional to the average phonon number. Consequently, from the result shown in Fig. 6(c), we can infer that even within the framework of conventional transport theory, the linear temperature dependence of metallic intrinsic resistivity occurs from a critical temperature lower than T_D.

There is no need for such a critical temperature to be much larger than T_D.

The percentage contributions of each phonon mode to the total intrinsic resistivity are shown in Table I, and the percentage contributions of AP and OP modes to the total intrinsic resistivity are shown in Fig. 6(d). We find that at low temperatures (<250 K), the intrinsic resistivity contributed by AP is much greater than that contributed by OP. This is because OP modes have higher energy than AP modes and are not easily thermally excited at low temperature. Therefore, in the low-temperature region from 70 to 250 K, the contribution of AP to intrinsic resistivity dominates. The spectral functions of AP and OP modes are shown in Fig. 6(e). We can see that the spectral functions of AP and OP are almost separated in frequency with very small overlap. Such a result is consistent with the phonon dispersion as shown in Fig. 2(b), where the frequency of AP looks globally lower than that of OP along the high-symmetry line. Based on these numerical results shown in Figs. 6(d) and 6(e), we conclude that the intrinsic resistivity in the range of 70–250 K is mainly contributed by the AP modes. In other words, we can disregard the OP modes in such a low-temperature region. And if we substitute $\alpha^2F_T^{AP}$ for α^2F_T to calculate the intrinsic resistivity, the numerical result does not change very much, in comparison with that shown in Fig. 5(b). As mentioned above, in the temperature region of 70–250 K, the ρ-T relation is dominated by the function $\mathcal{F}(T/T_0)$. Now that the OP modes are frozen, k_BT_0 can be understood as the maximal frequency of AP. From
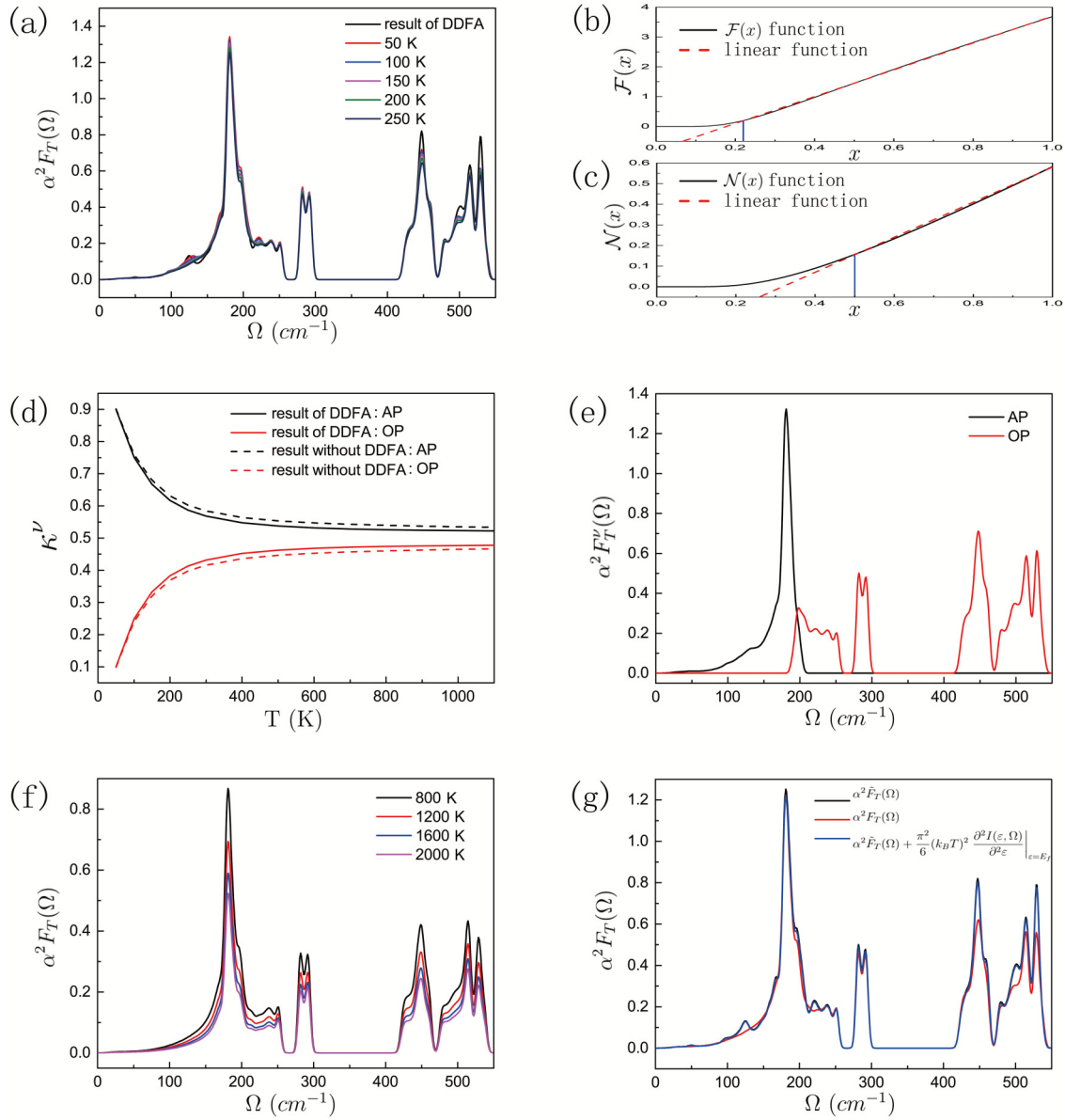
FIG. 6. (a) The spectral function $\alpha^2\tilde{F}_T(\Omega)$ and $\alpha^2F_T(\Omega)$ at temperatures of 50–250 K. (b) The plot of the function $\mathcal{F}(T/T_0)$. When the argument $x < 0.22$, the function $\mathcal{F}(T/T_0)$ begins to deviate from a linear function. (c) The plot of the function $\mathcal{N}(T/T_0)$. When the argument $x < 0.5$, the function $\mathcal{F}(T/T_0)$ begins to deviate from a linear function. (d) The percentages of the intrinsic resistivity contributed by AP (black line) and OP (red line) at different temperatures. The solid line represents the result calculated by $\alpha^2\tilde{F}_T(\Omega)$, the dashed line represents the result calculated by $\alpha^2F_T(\Omega)$. (e) The contributions of AP (black line) and OP (red line) to $\alpha^2F_T(\Omega)$ at $T = 100$ K. (f) The spectral function $\alpha^2F_T(\Omega)$ at temperatures of 800–2000 K. (g) The spectral function $\alpha^2\tilde{F}_T(\Omega)$, $\alpha^2F_T(\Omega)$, and $\alpha^2\tilde{F}_T(\Omega) + \frac{\pi^2}{6}(k_BT)^2 \frac{\partial^2I(\varepsilon,\Omega)}{\partial^2\varepsilon}\big|_{\varepsilon=E_f}$ at 300 K.

Fig. 6(e) we know that T_0 is about 300 K. According to our analysis about the function profile of $\mathcal{F}(T/T_0)$, the linear temperature dependence occurs from $0.22 \times 300 = 66$ K, in agreement with the numerical results shown in Fig. 5(b). In short, the first linear temperature dependence region from 70 to 250 K of Ti$_2$N originates from the AP modes. According to

TABLE I. Percentage of the contributions of each phonon mode to the intrinsic resistivity of Ti$_2$N at room temperature (300 K) calculated by α^2F_T and $\alpha^2\tilde{F}_T$, respectively. ρ^1–ρ^3 represent the contributions of the acoustic modes, and ρ^4–ρ^9 represent the contributions of the optical modes.

	ρ^1 (%)	ρ^2 (%)	ρ^3 (%)	ρ^4 (%)	ρ^5 (%)	ρ^6 (%)	ρ^7 (%)	ρ^8 (%)	ρ^9 (%)
α^2F_T	23.22	15.75	19.45	9.26	8.26	7.54	8.16	4.39	3.97
$\alpha^2\tilde{F}_T$	22.79	15.09	18.96	10.12	7.78	7.41	8.66	4.82	4.37

the Ziman formula, the linear temperature dependence starts to occur from a critical temperature as low as one-fifth of the maximal frequency of AP.

When $T > 250$ K, the OP modes start to play a role that ends the linear temperature dependence established by AP modes. Such a situation is demonstrated by the numerical result shown in Fig. 5(b) in the temperature range between 250 and 1400 K. However, if we employ the transport spectral function $\alpha^2 \tilde{F}_T$, which is completely independent of temperature due to the DDFA, the temperature dependence of the intrinsic resistivity arises exclusively from the function $\mathcal{F}(T/T_0)$. Just following the preceding analysis, we can find that the intrinsic resistivity even with the OP scattering incorporated has a linear temperature dependence from the critical temperature $0.22T_D = 172$ K, which is lower than the upper limit of the first linear ρ-T region established by AP scattering as shown in Fig. 5(b). Therefore, the DDFA always gives the linear ρ-T relation in the wide range from 70 to 2000 K as shown in Fig. 5(c). However, such a result is incorrect. As seen in Fig. 5(b), the temperature dependence of the spectral function $\alpha^2 F_T(\Omega)$ modifies the ρ-T spectrum drastically. In particular, the nontrivial temperature dependence of the spectral function in the temperature range from 250 to 1400 K, as shown in Fig. 6(f), has the linear temperature dependence of the intrinsic resistivity broken down. This result indicates that the spectral function in the DDFA is inappropriate for calculating the intrinsic resistivity in a relatively high-temperature range. In addition, $\alpha^2 \tilde{F}_T(\Omega)$, $\alpha^2 F_T(\Omega)$, and $\alpha^2 \tilde{F}_T(\Omega) + \frac{\pi^2}{6}(k_B T)^2 \frac{\partial^2 I(\varepsilon, \Omega)}{\partial^2 \varepsilon}|_{\varepsilon = E_f}$ at 300 K are plotted in Fig. 6(g). It can be seen that there is an obvious difference between $\alpha^2 \tilde{F}_T(\Omega)$ and $\alpha^2 F_T(\Omega)$, while the difference between $\alpha^2 \tilde{F}_T(\Omega)$ and $\alpha^2 \tilde{F}_T(\Omega) + \frac{\pi^2}{6}(k_B T)^2 \frac{\partial^2 I(\varepsilon, \Omega)}{\partial^2 \varepsilon}|_{\varepsilon = E_f}$ is not appreciable. This result indicates that the temperature correction contributed by the term of the Sommerfeld expansion, i.e., from the third to the last step of Eq. (6), is not the main reason for the difference between $\alpha^2 \tilde{F}_T(\Omega)$ and $\alpha^2 F_T(\Omega)$. Instead of that, the approximation from the second to the third step of Eq. (6) brings about the critical error of the DDFA. Therefore, the conditions $E_f \gg k_B T$ and $E_f \gg k_B T_D$ for the applicability of the DDFA are suspicious in monolayer Ti$_2$N due to the small electron and hole pockets as shown Fig. 2.

Our main conclusion is that the temperature dependence of the transport spectral function for e-ph scattering plays an important role in the intrinsic resistivity of such materials with the Fermi energy very close to the band edge. And we draw such a conclusion from the theoretical analysis on the Ziman formula and the transport spectral function presented in the Sec. II. Ti$_2$N monolayer is just a typical material to demonstrate such a conclusion by numerical calculations. Our recent theoretical investigations indicate that the DDFA also fails to describe quantitatively the intrinsic resistivity of plumbene (a kind of 2D plumbum material fabricated experimentally much recently) and some heavily doped semiconductors because a common feature of these materials is that they all have a Fermi level very close to the band edge. More details will be reported in our future work. What we would like to emphasize is that these theoretical results verify further our main conclusion in this work. In particular, our study indicates that when employ-

TABLE II. The values of the intrinsic resistivity of graphene, Ti$_3$C$_2$, Ti$_2$N, Nb$_4$C$_3$, and Ti$_2$C at room temperature (300 K).

Material	Resistivity ($\mu\Omega$ cm)
graphene	2[Ref. [5]]
Ti$_3$C$_2$	154[Ref. [30]]
Ti$_2$N	163
Nb$_4$C$_3$	460 000[Ref. [31]]
Ti$_2$C	6 800 000[Ref. [32]]

ing the Ziman formula to study the carrier mobility of doped semiconductors, one must take the temperature dependence of the transport spectral function into account since the Fermi energy is often very close to the band edge for the case of heavy doping. A systematical measure on the intrinsic resistivity of plumbene as a function of temperature is expected to give an experimental demonstration of our conclusion. Before ending our work, we remark briefly on the intrinsic resistivity of Ti$_2$N monolayer in comparison with other typical two-dimensional materials. As shown in Table II, the intrinsic resistivity of Ti$_2$N monolayer is higher than that of graphene by almost two orders of magnitude. However, its intrinsic resistivity is much lower than most other materials in the MXenes family. For example, the experimental measure of the intrinsic resistivity of Ti$_3$C$_2$ monolayer is about 154 $\mu\Omega$ cm, which is perhaps the lowest value among the MXenes materials available experimentally thus far [11]. Our numerical calculation indicates that the intrinsic resistivity of Ti$_2$N at room temperature is about 163 $\mu\Omega$ cm, comparable to that of Ti$_3$C$_2$ monolayer. This suggests that Ti$_2$N is a potential material with high conductivity.

IV. CONCLUSIONS

Within the theoretical framework of Ziman resistivity formula, the transport spectral function of e-ph interaction is the critical quantity for calculating the intrinsic resistivity of metals. Such a spectral function in the DDFA is extensively employed to calculate the intrinsic resistivity of metallic materials in recent works of first-principles calculations. In contrast, a more fundamental transport spectral function with the Fermi smearing effect due to finite temperature and nonzero phonon frequency is less involved. In this work, the validity of the DDFA as is used to calculate the intrinsic resistivity has been addressed. We find that the applicability of the DDFA requires the following: The Fermi energy must be far larger than the thermal excitation energy and the phonon Debye energy. In addition, a function incorporating the electronic density of states, the electron-phonon interaction matrix element, and the large-angle scattering weight must be slowly varying around the Fermi energy. However, it is not straightforward to identify whether the DDFA is applicable for realistic materials with a multisheet Fermi surface formed by several bands. To exemplify such an issue, we perform first-principles calculations of the intrinsic resistivity of Ti$_2$N monolayer, a kind of MXenes, by employing the two kinds of spectral functions. By comparison, we find that the spectral function with the DDFA fails to describe correctly the temperature dependence of the intrinsic resistivity of Ti$_2$N

monolayer when $T > 250$ K, much lower than the Debye temperature. The underlying physical reason is that some band edges are very close to the Fermi surface. On the other hand, the edges of other bands are far from the Fermi surface. But all of these bands span the Fermi level. In such a context, it is difficult to identify whether the Fermi energy is large enough for the applicability of the DDFA. Our results suggest that the spectral function with the Fermi smearing effect is always adequate for studying the intrinsic resistivity of realistic materials on the level of first-principles calculations. In contrast, the validity of the DDFA for realistic materials, particularly those materials with a complicated Fermi surface, should be given a great deal of attention before it is employed for numerical calculations. In addition, we remark briefly on the intrinsic resistivity of Ti_2N monolayer, in contrast to other typical two-dimensional materials, which is significant from the viewpoint of application of such an MXene material.

ACKNOWLEDGMENTS

[1] J. Bardeen and D. Pines, Phys. Rev. **99**, 1140 (1955).

[2] J. M. Ziman, *Electrons and Phonons: The Theory of Transport Phenomena in Solids* (Clarendon, Oxford, 1960).

[3] A. Giri, M. V. Tokina, O. V. Prezhdo, and P. E. Hopkins, Mater. Today Phys. **12**, 100175 (2020).

[4] Q. Tang, L. A. Svyatkin, and I. P. Chernov, Phys. Rev. B **99**, 205152 (2019).

[5] C.-H. Park, N. Bonini, T. Sohier, G. Samsonidze, B. Kozinsky, M. Calandra, F. Mauri, and N. Marzari, Nano Lett. **14**, 1113 (2014).

[6] D. Kim, Q. Li, P. Syers, N. P. Butch, J. Paglione, S. Das Sarma, and M. S. Fuhrer, Phys. Rev. Lett. **109**, 166801 (2012).

[7] L. Chen, X. Shi, N. Yu, X. Zhang, X. Du, and J. Lin, Materials **11**, 1701 (2018).

[8] D. B. Tanner and D. C. Larson, Phys. Rev. **166**, 652 (1968).

[9] F. Bloch, Z. Phys. **59**, 208 (1930).

[10] S. Baroni, S. de Gironcoli, A. Dal Corso, and P. Giannozzi, Rev. Mod. Phys. **73**, 515 (2001).

[11] B. Anasori, M. R. Lukatskaya, and Y. Gogotsi, Nat. Rev. Mater. **2**, 16098 (2017).

[12] Y. Li, Y. Guo, W. Chen, Z. Jiao, and S. Ma, J. Mater. Sci. **54**, 493 (2019).

[13] M. Khazaei, M. Arai, T. Sasaki, C.-Y. Chung, N. S. Venkataramanan, M. Estili, Y. Sakka, and Y. Kawazoe, Adv. Funct. Mater. **23**, 2185 (2013).

[14] H. Pan, J. Mater. Chem. A **3**, 21486 (2015).

[15] J. Guo, H. Fu, G. Zou, Q. Zhang, Z. Zhang, and Q. Peng, J. Alloys Compd. **684**, 504 (2016).

[16] I. R. Shein and A. L. Ivanovskii, Comput. Mater. Sci. **65**, 104 (2012).

[17] Y. Xie and P. R. C. Kent, Phys. Rev. B **87**, 235441 (2013).

[18] M. Khazaei, A. Ranjbar, M. Ghorbani-Asl, M. Arai, T. Sasaki, Y. Liang, and S. Yunoki, Phys. Rev. B **93**, 205125 (2016).

[19] U. Yorulmaz1, A. Özden1, N. K. Perkgöz, F. Ay, and C. Sevik, Nanotechnology **27**, 335702 (2016).

[20] P. B. Allen, Phys. Rev. B **13**, 1416 (1976).

[21] P. B. Allen, Phys. Rev. B **17**, 3725 (1978).

[22] Z. Liu, M. Zhu, and Y. Zheng, Phys. Rev. B **100**, 045145 (2019).

[23] P. B. Allen and B. Mikovic, in *Solid State Physics*, edited by H. Ehrenreich, F. Seitz, and D. Turnbull (Academic, New York, 1982), Vol. 37.

[24] P. Giannozzi, O. Andreussi, T. Brumme, O. Bunau, M. B. Nardelli, M. Calandra, R. Car, C. Cavazzoni, D. Ceresoli *et al.*, J. Phys.: Condens. Matter **29**, 465901 (2017).

[25] N. Troullier and J. L. Martins, Phys. Rev. B **43**, 1993 (1991).

[26] J. P. Perdew, K. Burke, and M. Ernzerhof, Phys. Rev. Lett. **77**, 3865 (1996).

[27] J. D. Pack and H. J. Monkhorst, Phys. Rev. B **16**, 1748 (1977).

[28] S. Poncé, E. R. Margine, C. Verdi, and F. Giustino, Comput. Phys. Commun. **209**, 116 (2016).

[29] N. W. Ashcroft and N. David Mermin, *Solid State Physics* (Thomson Learning, Ithaca, 1976).

[30] A. D. Dillon, M. J. Ghidiu, A. L. Krick, J. Griggs, S. J. May, Y. Gogotsi, M. W. Barsoum, and A. T. Fafarman, Adv. Funct. Mater. **26**, 4162 (2016).

[31] M. Ghidiu, M. Naguib, C. Shi, O. Mashtalir, L. M. Pan, B. Zhang, J. Yang, Y. Gogotsi, S. J. L. Billingebd, and M. W. Barsoum, Chem. Commun. **50**, 9517 (2014).

[32] M. Naguib, O. Mashtalir, J. Carle, V. Presser, J. Lu, L. Hultman, Y. Gogotsi, and M. W. Barsoum, ACS Nano **6**, 1322 (2012).